POSITRON EMISSION TOMOGRAPHY IN SOLID STATE PHYSICS*

G. Kontrym-Sznajd

Institute of Low Temperature and Structure Research, Polish Academy of Sciences
P.O. Box 1410, 50-950 Wrocław 2, Poland

(Received August 21, 2017)

Measurements of electron–positron annihilation rays have found applications in both a medical diagnosis and in solid state physics. A similar equipment, located either close to or far from an investigated object, allows to study some quantities either in the real or momentum space — medical or physical investigations, respectively. In the paper, various mathematical methods of computed tomography and their applications to objects having the cubic and hexagonal symmetry are presented, showing some examples of electron–positron momentum densities, which visualize the Bloch states of the electron wave function.

DOI:10.5506/APhysPolB.48.1601

1. Introduction

The phenomenon of a low-energy positron–electron annihilation have found applications in both a medical diagnostics and in a solid state physics [1]. Since the probability of electron–positron (e–p) annihilation with emitting n quanta γ is proportional to $(1/137)^n$, in the case of antiparallel spins of annihilating particles, the most probable is the 2γ process. Conservations laws cause that if the momentum $\boldsymbol{p}$ of the e–p pair is equal to zero, generated 2γ rays are antiparallel, each one with the momentum mc (m — electron mass, c — light speed), while for $|p| \neq 0$, there is a distortion from the colinearity. However, because $|p| \ll mc$, this distortion is very small, *e.g.* electrons inside the central Fermi surface (FS) are observed for angles lower than 0.3° (see explanations in [2]). Thus, if counters are located close to investigated object (medical PET), one obtains information on a positron localization (real space $\boldsymbol{r}$), while after moving counters far from

* Presented at the 2nd Jagiellonian Symposium on Fundamental and Applied Subatomic Physics, Kraków, Poland, June 3–11, 2017.

the sample, one measures the angular correlation of annihilation radiation (ACAR) which probes the e–p momentum density, $\rho(\boldsymbol{p})$, in the extended $\boldsymbol{p}$-space. $\rho(\boldsymbol{p})$, being crucial in understanding electronic properties of quantum systems, is defined as

$$\rho(\boldsymbol{p}) = \sum_{\boldsymbol{k}j} n_{\boldsymbol{k}j} \delta(\boldsymbol{p} - \boldsymbol{k} - \boldsymbol{G}) \left| \int_{-\infty}^{\infty} e^{-i\boldsymbol{p}\cdot\boldsymbol{r}} \Psi_{\boldsymbol{k}j}(\boldsymbol{r}, \boldsymbol{r}) \mathrm{d}\boldsymbol{r} \right|^2 , \tag{1}$$

where $\Psi_{\boldsymbol{k}j}(\boldsymbol{r}_e, \boldsymbol{r}_p)$ and $n_{\boldsymbol{k}j}$ are, respectively, the e–p wave function and the occupation number of an electron state $\boldsymbol{k}$ in the j^{th} band, $\boldsymbol{G}$ is the reciprocal lattice vector. Momentum $\boldsymbol{k}$ extends over the first Brillouin zone, so-called reduced zone.

$\rho(\boldsymbol{p})$ can be measured via its single or double integrals (line (2D ACAR) or plane (1D ACAR) projections, respectively) [3, 4] or even directly by simultaneously measuring 2D ACAR and energies of 2γ rays [5]. Studying projections along different integration directions, 3D densities $\rho(\boldsymbol{p})$ can be reconstructed from 1D or 2D ACAR spectra (abbreviation nD (1D, 2D, 3D) denotes n-dimensional).

The problem of image reconstruction from projections came into being independently in various scientific fields from radio astronomy, geology, physics or biology to medical diagnostics. Its mathematical solution was proposed already in 1917 by Radon [6], who considered a real function in the N-dimensional space and its integrals over $(N-1)$-dimensional hyperplanes. Radon provided a formula for the inverse transform (named the Radon transform), which has many applications to partial differential equations [7]. Mathematical methods used for reconstructing $\rho(\boldsymbol{p})$ from ACAR spectra are described in Section 3.

2. Electronic structure studied by positrons

For studying the electronic structure of crystalline solids, particularly the FS, different experimental techniques are used. Some of them, so-called magnetic or quantum oscillatory techniques [8], allow to estimate only some quantities related to the FS. Moreover, they are restricted to both low temperatures and high-purity samples. Meanwhile, non-magnetic methods, as angle resolved photoemission spectroscopy (ARPES), ACAR or Compton scattering [9], which do not have such restrictions, yield information on the shape of the FS in arbitrary points of the reciprocal space. Of course, they have other limitations — see remark denoted as Ref. [2] and comments in [3, 4, 10].

The FS topology, related to many material properties, is responsible for variety of exotic phenomena as, *e.g.*, unconventional superconductivity [11, 12], magnetism in the heavy rare earths [13], spin density waves or

other phenomena which accompany quantum criticality [14, 15]. Positrons annihilation and Compton scattering are used in such studies from the beginning — the first experiment, which showed the webbing of the FS with corresponding size of the webbing vector, linked with the magnetic ordering, was just 2D ACAR experiment in Y [16].

ACAR and Compton scattering probe the FS via e–p and electron momentum density $\rho(\boldsymbol{p})$ in the extended space $\boldsymbol{p}$, respectively. This density, defined in Eq. (1), contains unique information [17] — not only on the occupied momentum states (and hence the FS) but also on the electron wave functions. It shows that in the periodic lattice, electron and positron wave functions are the Bloch function and

$$\rho(\boldsymbol{p} = \boldsymbol{k} + \boldsymbol{G}) = \sum_{\boldsymbol{k}j} n_{\boldsymbol{k}j} \left| A_{\boldsymbol{k}j} \right|^2 \delta(\boldsymbol{p} - \boldsymbol{k} - \boldsymbol{G}) \tag{2}$$

what means that in each band j, there is a "leading" term of the density and the so-called "Umklapp" or higher momentum components (HMC) — see Fig. 1, in which experimental 2D ACAR spectra for silver and quartz are displayed.

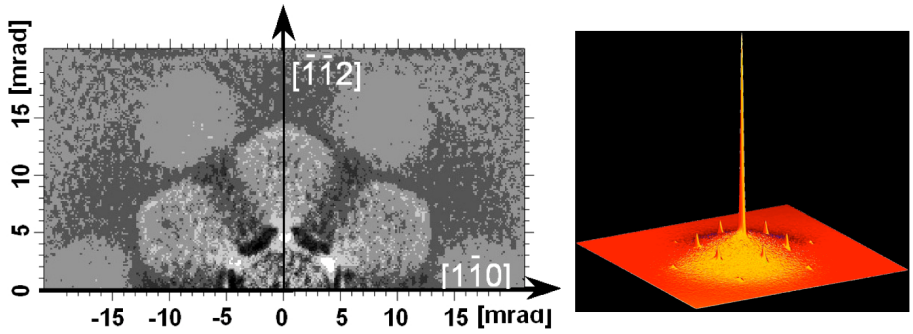

Fig. 1. Anisotropic part of experimental 2D ACAR spectra for silver with p_x along [111] [17] and 2D ACAR data for α-quartz (in the range of $|p|$ up to 15 mrad) with p_x along the hexagonal [001] axis [18] — left and right parts, respectively.

In the case of silver, the isotropic average of 2D ACAR spectrum was subtracted in order to visualize the anisotropy of the FS (neck in [111]) and the 1$^{\text{st}}$ and 2$^{\text{nd}}$ HMCs. The spectrum for quartz [18] contains two contributions: one coming from para-positronium (a hydrogen-like e–p bound state) and the second one (much broader) which comes from free positron annihilation. Since the positronium is itself thermalized before annihilation, its momentum distribution will be very narrow which at finite resolution looks like a very sharp peak at zero momentum. There are also Umklapp contributions at the reciprocal lattice vectors, which demonstrates that para-positronium

also propagates in the Bloch states. Its sharp shape illustrates a high quality of the 2D ACAR spectrometer after replacing the Anger camera by the new HIDAC system [19] — see Fig. 3 in [18].

3. Reconstruction techniques

We discuss techniques used both in a medical tomography and in reconstructing e–p momentum densities $\rho(\boldsymbol{p})$ from 2D ACAR data, *i.e.* from line projections of $\rho(\boldsymbol{p})$

$$N(p'_y, p'_z) = \int_{-\infty}^{\infty} \mathrm{d}p'_x \rho(\boldsymbol{p})\,, \tag{3}$$

where (p'_x, p'_y, p'_z) denotes rectangular system connected with the equipment.

Mathematical solutions of Eq. (3) can be classified into two categories: (1) series expansions, known as algebraic reconstruction techniques (ART) [20], in which integral (3) is reduced to the sum; (2) transform methods [21], which consist in various analytical inversion of the Radon transform. Because ART algorithms require much more memory and computation time than transform methods, for a long time they have not been used in both medical and ACAR experiments imaging.

In transforms methods, the reconstruction of 3D densities is reduced to a set of reconstructions of 2D densities, performed independently on the succeeding parallel planes. The exception is Pecora's method [22, 23] in which for each 2D spectrum, one estimates some number of 1D spectra to apply a reconstruction algorithm for plane projections [3].

To the first 2D ACAR measurements, until the year 1989 [3], similarly as in a medical imagine, the filtered back-projection (FBP) technique had been applied. When the computing power increased, more advanced methods were introduced, however still from the group of the transform methods: the fast Fourier transform (FFT) [24] and Cormack's method (CM) [25], being multiply applied to 2D ACAR data (Refs. [17–32] (CM) and [63–82] (FFT) cited in [3]). As concerns a system of linear equations, in principle, it could be solved by the matrix inversion. However, because of its high dimensionality, ART are based on the iterative algorithms with using optimisation methods, *e.g.* quadratic or entropy optimisation and Bayesian analysis. For the first time, such a technique (with using Maximum Entropy Method (MEM) [26]) was applied to 2D ACAR data for Gd [27].

Recently, the Munich 2D ACAR spectrometer at the Maier-Leibnitz accelerator laboratory in Garching has been launched. The first measurements were performed on Cr [28] in the antiferromagnetic and paramagnetic phases and on Cu [29]. For Cu, three 2D ACAR spectra were measured and 3D $\rho(\boldsymbol{p})$ were reconstructed using MEM with taking into account the full symmetry

of the reciprocal lattice, *i.e.* performing reconstruction of 3D density in the whole space at the same time instead of independently on 2D planes. In the next paper [30], devoted to studying the FS of the localized ferromagnetic Heusler compound with using spin-polarized positrons, the authors introduced into the MEM both the experimental resolution and the noise. Here, we would like to notice that all these is also done within the MEM proposed for reconstructing densities from both plane [31] and line [26] projections, applied to Gd [27]. However, because of the hcp symmetry of Gd, where on each of the planes, perpendicular to the c axis, points $\boldsymbol{p}$ are independent, the most sensible is to perform reconstructions on each of 2D planes independently. The similar remark concerns tetragonal and trigonal structures — here only the cubic structures, having three axis of the highest order, make an exception. Of course, when one performs reconstruction on 2D planes, one should deconvolute experimental spectra before reconstructing $\rho(\boldsymbol{p})$, what was just done for Gd data [27] (within procedure [32]).

Of course, reconstructed 3D densities always must have the full 3D symmetry of the reciprocal space (or crystal in the case of studying quantities in the real space). For the cubic symmetries, if the reconstruction is performed independently on 2D planes, perpendicular to [001] direction (*i.e.* the cubic symmetry is treated as a structure with one rotation axis of the 4^{th} order), it is done by imposing (on reconstructed 3D $\rho(\boldsymbol{p})$) the symmetry requirement [33] (see Fig. 2)

$$\rho\left(p_x, p_y, p_z\right) = \rho\left(p_y, p_z, p_x\right) = \rho\left(p_x, p_z, p_y\right) . \tag{4}$$

The symmetry requirement can be also introduced via expanding reconstructed densities into the cubic harmonics. This particular algorithm (rather complicated and time consuming), applied to both models and 2D ACAR experimental data in LaB_6 [33], not only filters the experimental noise but also enhances some details of the reconstructed densities. Thanks to such a procedure, it was possible to reproduce a very small element of the FS in LaB_6, not seen when applying, to the same experimental data, either FBP or CM.

The ART method used in [28–30] and [34] with a parametrization of the FS treated explicitly during the reconstruction (instead of determined afterwards from the reconstructed densities as done by others) is described in detail in Refs. [35, 36].

In Fig. 3, model densities reconstructed from line projections via the ART (with a simple iteration) and FBP procedure are compared. As can be seen, the ART gives much better results. In this particular case, the CM gives similar results to FBP, which is not surprising because this model density

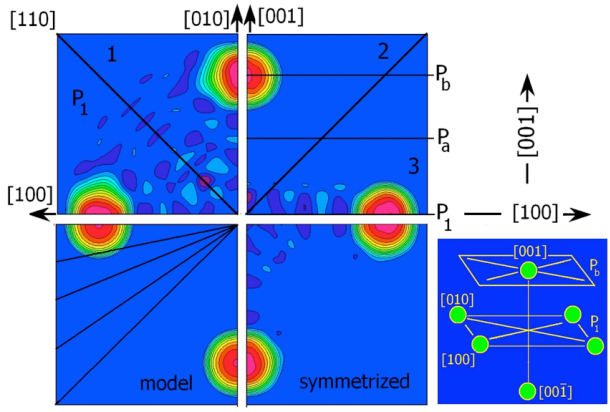

Fig. 2. Densities reconstructed from five model projections ([100], [110] and three between), marked in the left, lower part of the figure. Upper part: densities on the first plane P_1, perpendicular to [001] (left part) and along [100] direction on succeeding parallel planes (*e.g.* P_a, P_b). Lower right part shows densities after applying the symmetry requirement (Eq. (4)), *i.e.* after averaging results in areas numbered by 1 to 3 in the upper part.

is very sharp-edged, thus it is difficult to be described by a finite polynomials series. This is the reason that the CM (and other techniques using expansion into orthonormal polynomials) was never used in medical imaging.

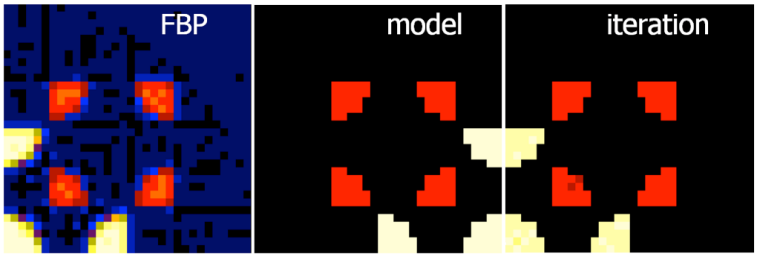

Fig. 3. Model density reconstructed by the ART and FBP procedures [37].

What could be expected under applying such techniques to real e–p momentum densities? Results for Gd (with using MEM and CM) [27] showed that both methods give very similar results with a little supremacy of MEM, which, though, was much more time consuming.

In the chapter "Overview of reconstruction methods" (page 82 in [36]), Weber compares ART with other algorithms belonging to the transform methods. Because discussed questions are important and perhaps they require additional research, I discuss some of them.

1. *It is not possible to incorporate the full crystalline symmetry with the CM, as only 2D slices are reconstructed.* This is true but only for the cubic structures. However, for the cubic structures, the full crystalline symmetry could be imposed on the reconstructed 3D densities via Eq. (4) — see the text below and after Eq. (4).

2. *The CM is not suited very well to detect the sharp discontinuities of the Fermi breaks.* It takes place for very particular models, as *e.g.* presented in Fig. 3. It is not a case for real data when they represent e–p momentum densities which are smeared not only by the equipmental resolution but also via electron–electron correlations. Moreover, for sharp densities, one can apply two step reconstruction — see Fig. 4 and the text starting from the last paragraph on the page 1694 in [38].

3. *All the reconstruction methods mentioned above (i.e. transform method) have one thing in common: they are analytically exact if (i) the statistics is infinitely good, (ii) the resolution is homogeneous, (iii) the discretization of the measurement is infinitesimal small and (iv) an infinite number of projections is measured. In an ACAR measurement none of these requirements are fulfilled exactly.* In the CM, the expansion of data into orthogonal polynomials has the mean-squares approximation properties, which reduces experimental noise. As concerns point *(iv)* — on the contrary, one should measure only a few directions but with high statistic (this question is also discussed below in point 4). For example, in Gd (the same for Y [16]) for a proper description of projections four functions $g_n(p)$ are sufficient. Fifth function ($g_{24}(p)$) is of the order of the experimental noise — see Fig. 1 in [27] and Fig. 4 below, which shows that the fourth radial component of density has also very small values.

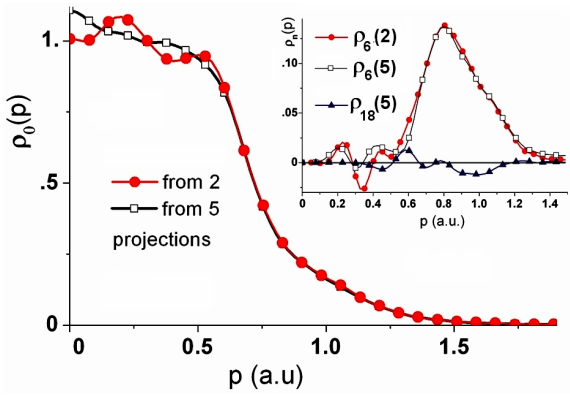

Fig. 4. Functions $\rho_n(p)$ in Y, in percent of $\rho_0(0)$, reconstructed either from two or five projections. The meaning of presented $\rho_n(p)$ is given in the figure, where the numbers in parentheses mean the numbers of projections used in the reconstruction.

4. *Using the ART, the quality of the reconstruction is always getting better the more information is used. In contrast, adding a projection with very low statistics can worsen the result of a reconstruction if done with DT, FBP or CM.* For each method, it is better when the more information is used. However, adding a projection at the cost of lowering statistic of other projections can worsen results — particularly for directions lying so close to each other that it is impossible to observe (in the limit of both low experimental statistics and resolution) differences between such spectra. This question is discussed in detail on pages 4 and 5 in [39].

4. Conclusions

Recent papers [26–30, 34–36] and results presented in Fig. 3 show that the ART algorithm is very promising, reproducing an image of much better quality than the FBP or other transform methods. To improve the quality of imaging, it is very beneficial to combine various reconstruction techniques — *e.g.* when the iteration is initialized by FBP. The full iterative reconstruction could model not only the noise statistics, but also the geometry of the equipment and other artifacts. This is particularly important in medical imaging because a significant improvement of picture quality creates an opportunity for reduction of radiation dose.

The latest innovations in commercial CT systems and evolution of reconstruction techniques, are described in [40]. In turn, in [41–46], the authors present new possibilities with the use of the Jagiellonian University PET (J-PET). It is the first PET scanner based on organic scintillators, which has to register, additionally, 3γ quanta from decays of the ortho-positronium (o-Ps) and its lifetime. Thanks to this, J-PET is also intended for basic research, for example, discrete symmetries (time delineation or CPT symmetry) in decay of positronium [45]. Moreover, authors plan to check if properties of the o-Ps, produced within cells, can be used as a diagnostic marker for determining the degree of a tumor progression. The use of positron annihilation lifetime spectroscopy (PALS) in cancer research is described in *e.g.* Refs. [47–49].

I am very grateful to Professors S.B. Dugdale and P. Moskal for their helpful remarks.

REFERENCES

[1] R.N. West, in: *Nuclear Physics Methods in Materials Research*, Proceedings of the Seventh Divisional Conference Darmstadt, pp. 234–247, Springer, 1980, ISBN 978-3-322-85996-9.

[2] $1^\circ \cong 17.5$ [mrad] where [mrad] $= 0.137$ [a.u.]$^{-1}$ (atomic units of momentum), denotes momenta in the units [10^{-3} mc $= 1$]. Because electrons inside the central FS are observed for angles $\Theta < 0.3^\circ$, only measurements with $\Delta\Theta$ at least 0.01° are reasonable. This requires a very long distance between detectors and sample what results in a significant lowering of experimental statistics. It is the reason for the ACAR experiment to be time consuming.

[3] G. Kontrym-Sznajd, *Low Temp. Phys.* **35**, 599 (2009). It should be noted that numbering of references in Table 1 in [3] contains some mistakes. They are properly written in `arXiv:0810.0641v2 [cond-mat.other]`.

[4] S.B. Dugdale, *Low Temp. Phys.* **40**, 328 (2014).

[5] C.S. Williams, L.W. Burggraf, P.E. Adamson, J.C. Petrosky, *Nucl. Instrum. Methods Phys. Res. A* **629**, 175 (2011).

[6] J. Radon, *Berichte Sachsische Akademie der Wissenschaften* **69**, 262 (1917).

[7] F. John, *Plane Waves and Spherical Means Applied to Partial Differential Equations*, Interscience, NY 1955.

[8] A. Carrington, *Rep. Prog. Phys.* **74**, 124507 (2011).

[9] *X-ray Compton Scattering*, (Eds.) M.J. Cooper, P.E. Mijnarends, N. Shiotani, N. Sakai, A. Bansil, Oxford University Press, Oxford 2004.

[10] T.D. Haynes *et al.*, *New J. Phys.* **14**, 035020 (2012).

[11] P. Fulde, R.A. Ferrell, *Phys. Rev.* **135**, A550 (1964); A.I. Larkin, Yu.N. Ovchinnikov, *Zh. Eksp. Teor. Fiz.* **47**, 1136 (1964) [*Sov. Phys. JETP* **20**, 762 (1965)].

[12] M.J. Winiarski, M. Samsel-Czekała, *J. Alloy. Compd.* **560**, 123 (2013).

[13] I.D. Hughes *et al.*, *Nature* **446**, 650 (2007).

[14] P. Gegenwart, Q. Si, F. Steglich, *Nature Physics Focus* **4**, 186 (2008).

[15] M.J. Winiarski, M. Samsel-Czekała, *Solid State Commun.* **179**, 6 (2014).

[16] S.B. Dugdale *et al.*, *Phys. Rev. Lett.* **79**, 941 (1997).

[17] G. Kontrym-Sznajd, H. Sormann, *Phys. Status Solidi B* **251**, 140 (2014).

[18] S.B. Dugdale *et al.*, *J. Phys.: Conf. Ser.* **443**, 012083 (2013).

[19] A.P. Jeavons, R.A. Chandler, C.A.R. Dettmar, *IEEE Trans. Nucl. Sci.* **46**, 468 (1999).

[20] G.T. Herman, A. Lent, *Comput. Biol. Med.* **6**, 273 (1976); G.T. Herman, L.B. Meyer, *IEEE Transactions on Medical Imaging* **12**, 600 (1993).

[21] G.T. Herman, *Image Reconstruction from Projections*, Academic, NY 1980; R.M. Lewitt, *Proc. IEEE* **71**, 390 (1983).

[22] L.M. Pecora, *IEEE Trans. Nucl. Sci.* **NS-34**, 642 (1987).

[23] L.M. Pecora *et al.*, *Phys. Rev. B* **37**, 6772 (1988).

[24] R. Suzuki, S. Tanigawa, in: *Positron Annihilation*, (Eds.) L. Dorikens-Vanpraet, M. Dorikens, D. Segers, World Sci., Singapore 1989, p. 626.

[25] A.M. Cormack, *J. Appl. Phys.* **34**, 2722 (1963); **35**, 2908 (1964).

[26] K.W. Fornalski *et al.*, *Acta Phys. Pol. A* **117**, 892 (2010).
[27] M. Pylak, L. Dobrzyński, G. Kontrym-Sznajd, *Appl. Phys. A* **104**, 587 (2011).
[28] H. Ceeh *et al.*, *J. Phys.: Conf. Ser.* **443**, 012094 (2013).
[29] J.A. Weber *et al.*, *J. Phys.: Conf. Ser.* **443**, 012092 (2013).
[30] J.A. Weber *et al.*, *Phys. Rev. Lett.* **115**, 206404 (2015).
[31] L. Dobrzyński, A. Holas, *Nucl. Instrum. Methods Phys. Res. A* **383**, 589 (1996).
[32] H.M. Fretwell *et al.*, *Europhys. Lett.* **32**, 771 (1995).
[33] G. Kontrym-Sznajd, M. Samsel-Czekała, M. Biasini, Y. Kubo, *Phys. Rev. B* **70**, 125103 (2004).
[34] J.A. Weber *et al.*, *Phys. Rev. B* **95**, 075119 (2017).
[35] M. Leitner, J.A. Weber, H. Ceeh, *New J. Phys.* **18**, 063033 (2016).
[36] J.A. Weber, Spin-polarized Positron Annihilation Spectroscopy. Investigation of Complex Metallic Systems, Ph.D. Thesis, Technische Universität München, 2017, `http://d-nb.info/112881935X/34`
[37] M. Biasini, G. Kontrym-Sznajd, *Materials Science Forum* **666**, 147 (2011).
[38] G. Kontrym-Sznajd, M. Samsel-Czekała, M. Biasini, *Appl. Phys. A* **91**, 131 (2008).
[39] G. Kontrym-Sznajd, *J. Appl. Cryst.* **48**, 11 (2015).
[40] D. Fleischmann, F.E. Boas, *Eur. Radiol.* **21**, 510 (2011).
[41] P. Moskal *et al.*, *Nucl. Instrum. Methods Phys. Res. A* **764**, 317 (2014).
[42] L. Raczyński *et al.*, *Nucl. Instrum. Methods Phys. Res. A* **786**, 105 (2015).
[43] D. Kamińska *et al.*, *Eur. Phys. J. C* **76**, 445 (2016).
[44] A. Gajos *et al.*, *Nucl. Instrum. Methods Phys. Res. A* **819**, 54 (2016).
[45] P. Moskal *et al.*, *Acta Phys. Pol. B* **47**, 509 (2016).
[46] P. Moskal *et al.*, *Phys. Med. Biol.* **61**, 2025 (2016).
[47] G. Liu *et al.*, *Phys. Status Solidi C* **4**, 3912 (2006).
[48] A.A. Pivtsaev, V.I. Razov, *J. Synch. Investig.* **10**, 816 (2016).
[49] E. Axpe *et al.*, *PLOS ONE* **9**, e83838 (2014).